Biophysical Journal, Volume *112*

Supplemental Information

Transient Thresholding: A Mechanism Enabling Noncooperative Transcriptional Circuitry to Form a Switch

Katherine H. Aull, Elizabeth J. Tanner, Matthew Thomson, and Leor S. Weinberger

Supporting Material

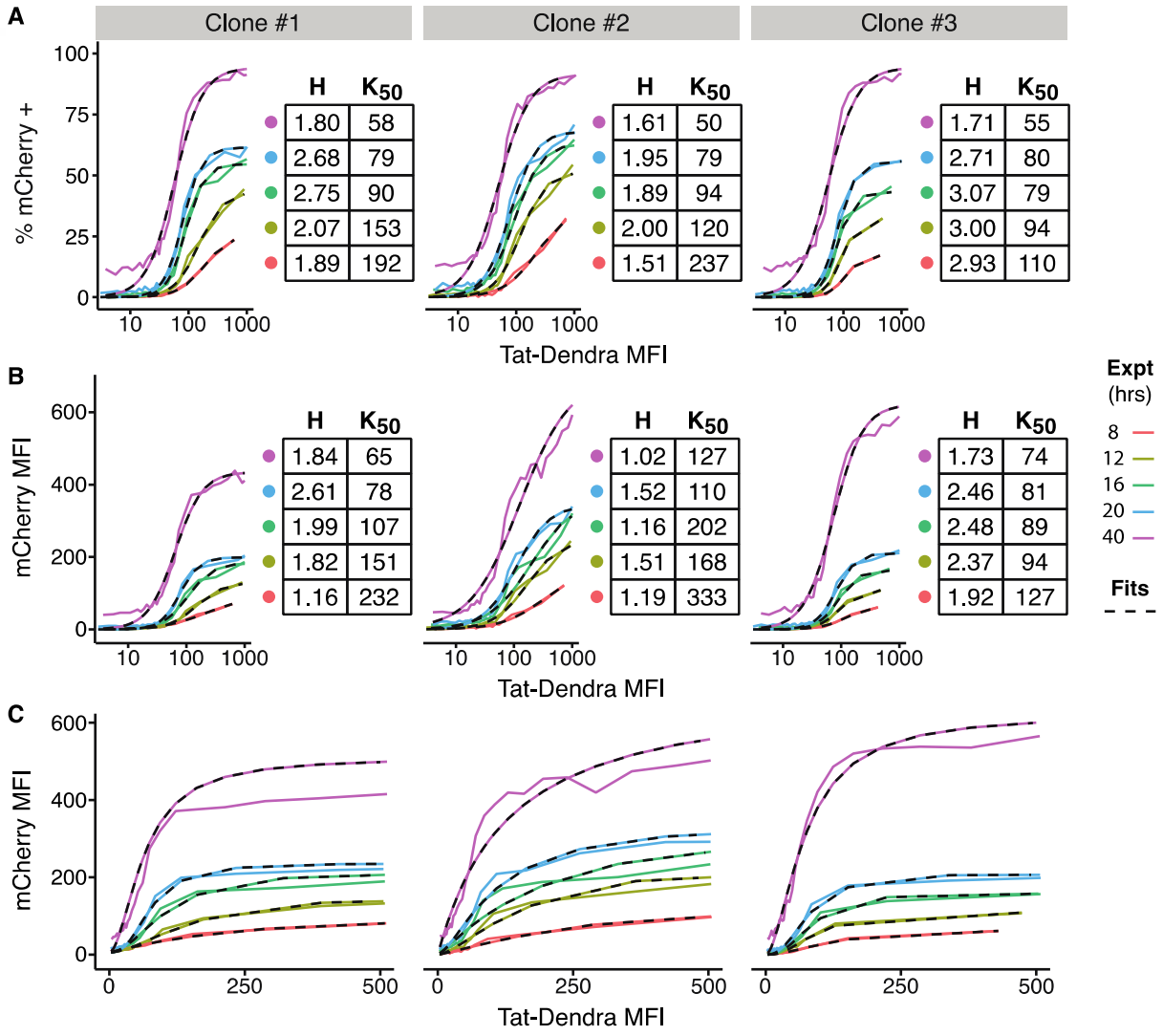

Figure S1: The open-loop Tat-LTR circuit exhibits a threshold in both activation and mean expression. (A) Flow data from three isoclones of Jurkat Tat-Dendra + LTR mCherry-deg cells, as shown in raw form in Fig. 2D and as dose-response plots in Fig. 2E, fit to a Hill function (Methods). The dose-response data and Hill fit lines are depicted for each condition, with Hill coefficient (*H*) and half-maximal binding (K_{50}) values in adjacent tables together with goodness of fit (R^2). (B) The equivalent dose-mean expression curves in Fig. 2E were analyzed as in panel A. (C) Data and fits from panel B, with Tat-Dendra on a linear scale to emphasize the weakly sigmoidal shape. All fits gave $R^2 > 0.96$.

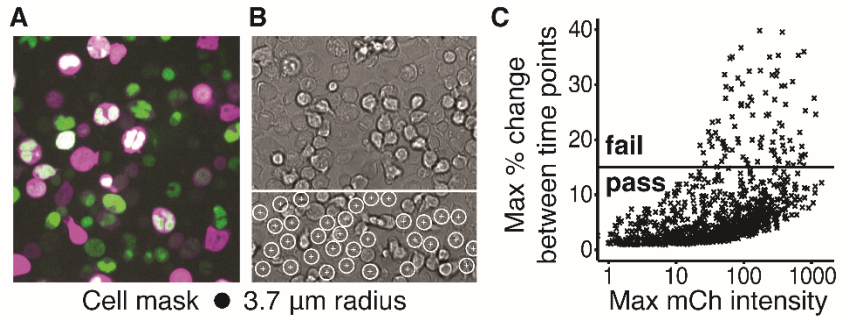

Figure S2: Extraction and QC of single-cell trajectories from time-lapse images. (A) Jurkat Tat-Dendra + LTR mCherry-deg cells underwent time-lapse microscopy to yield the data described in Fig. 3. Briefly, the cells were biotinylated, attached to a streptavidin-coated coverslip, then induced with 250 ng/mL Dox and imaged for 20 hours. Full details of this procedure are in Methods. This two-color fluorescence image is from the final time point of Clone #2, and shows one tile of a 5x5 grid. Tat-Dendra is green; mCherry is magenta. (B) The same location as (A), in brightfield. Cell locations were marked in brightfield to ensure that dim and non-fluorescent cells are fairly represented. The lower section of the image shows the marked cell centers (white +) surrounded by a 23-pixel diameter circle, which is taken as the cell's area. Pixels within this area contribute to the fluorescence intensity of the cell. This location is used for all time points to create a single-cell trajectory. (C) To reduce noise in the data, trajectories that showed excessive changes between consecutive time points were discarded. This image shows raw mCherry trajectories from Clone #2 undergoing QC. The maximum percent change between two consecutive time points is plotted as a function of maximum intensity, showing that for both dim and bright cells, most have a percent change under 10%. To pass QC, both Dendra and mCherry channels must be under the 15% noise cutoff shown. These raw trajectories underwent further QC, smoothing, and bleaching correction, as detailed in Methods and Fig. S3.

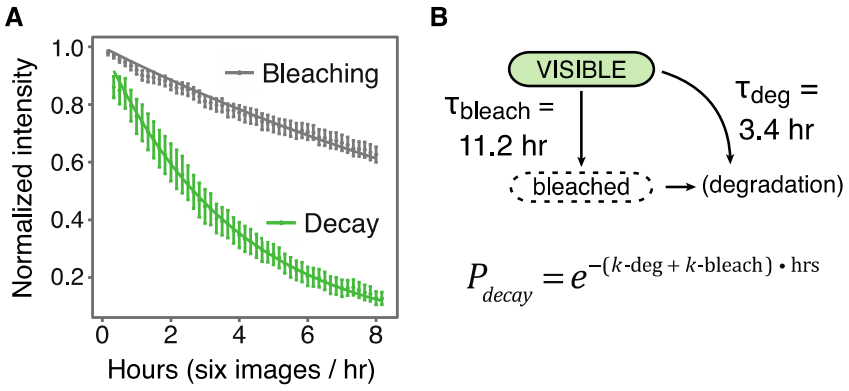

Figure S3: Correcting for photobleaching in Tat-Dendra trajectories. (A) Single-cell trajectories were constructed from time-lapse imaging of bright Jurkat Tat-Dendra cells. For the decay curve, cycloheximide was added at t=0 to stop protein synthesis, and images were taken every 10 minutes. For the bleaching curve, the same number of images was taken in 5-second intervals to simulate non-decaying protein. Error bars show 95% CI. (B) These trajectories were fit to simple exponential decay models. The bleaching half-time was measured at 11.2 hours. The total rate of visible protein decay can be expressed as the sum of the bleaching and degradation rates; from this equation, the half-life of Tat-Dendra was calculated at 3.4 hours. This value was confirmed by flow cytometry experiments (data not shown). To compute the amount of non-fluorescent protein present, we assume that a fraction of Tat-Dendra enters the bleached state at each time point, and the bleached protein degrades at the normal rate.

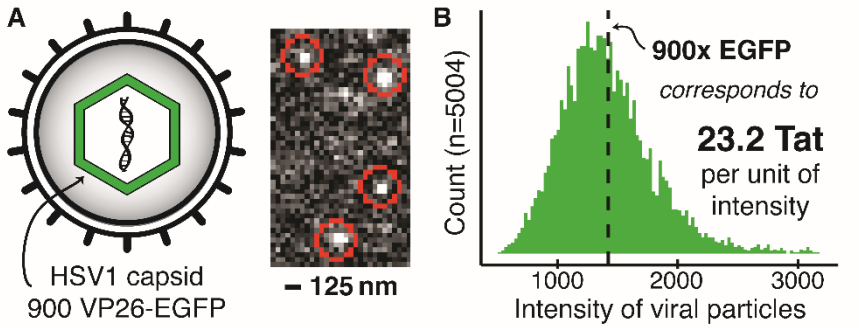

Figure S4: Quantitation of Tat-Dendra by HSV-GFP molecular standard. (A) HSV-GFP viral particles can serve as a "molecular ruler" to convert fluorescence intensity to molecular number. Since the HSV capsid protein VP26 is fused to EGFP, and each viral particle assembles into an icosahedron with precisely 900 copies of VP26, each viral particle contains 900 EGFP molecules. A small portion of a representative image of HSV-GFP is shown; diffraction-limited viral particles that were successfully segmented are circled in red. (B) Histogram of intensities from all viral particles (n=5004) that were identified, showing a roughly normal distribution with a mean of 1424 intensity units per particle. An increase of one intensity unit corresponds to 23.2 Tat-Dendra molecules; this conversion is detailed in Methods.

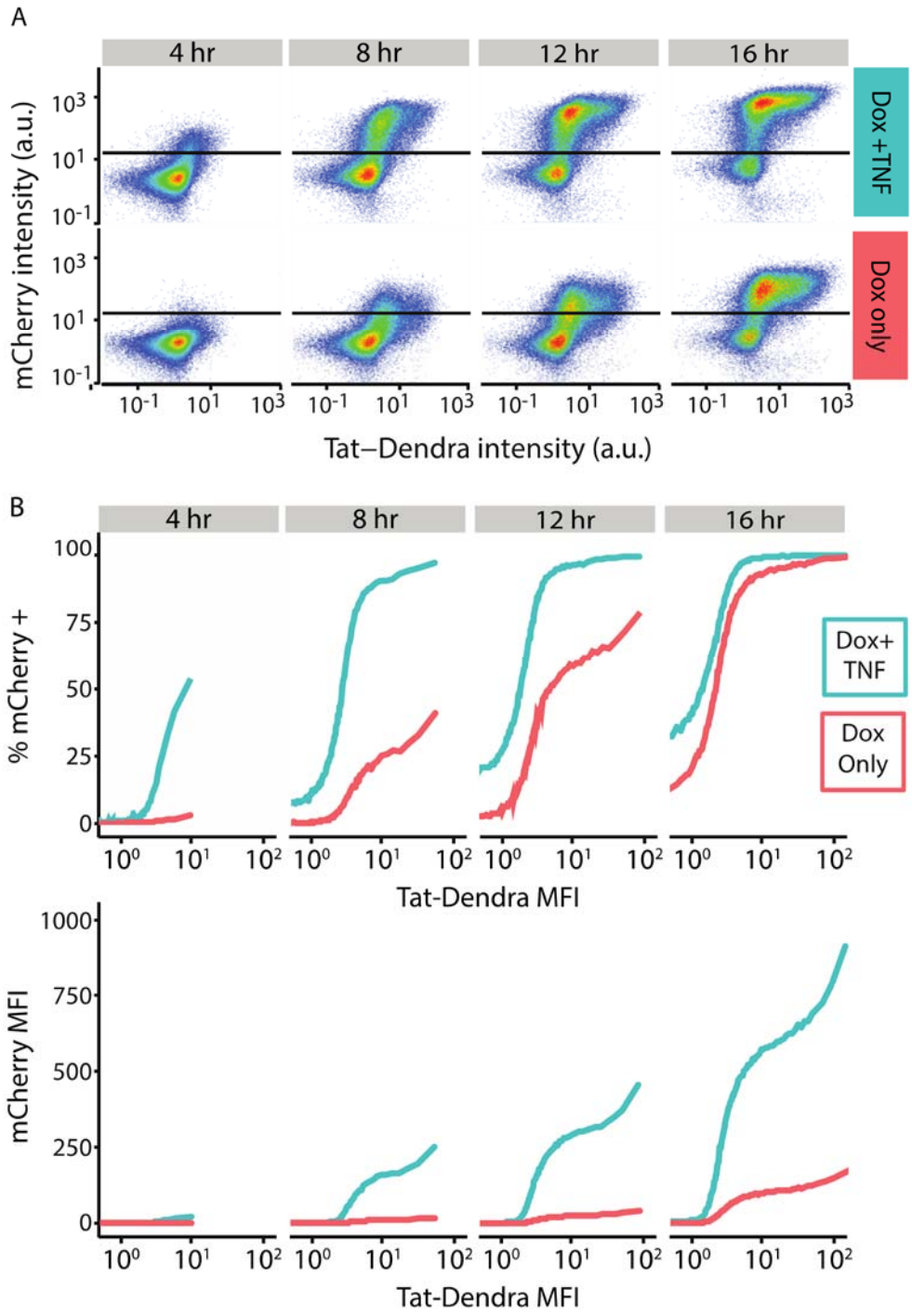

Figure S5: LTR activation by TNF shortens the lifetime of transient Tat-activation threshold. (A) Flow cytometry time-course (as in Fig 2) for Jurkat LTR isoclone #4. Horizontal line indicates the mCherry positive cutoff; 10,000 randomly sampled cells displayed. (B) Dose-response curves for % mCherry positive cells (top) and mCherry MFI (bottom) from data in panel A. Individual cells were ranked by Dendra intensity and sorted into 100 bins based on percentile. Each bin contained a minimum of 3,000 cells. Percentage of cells above the mCherry positive cutoff and median mCherry and Dendra fluorescence were calculated for each bin.

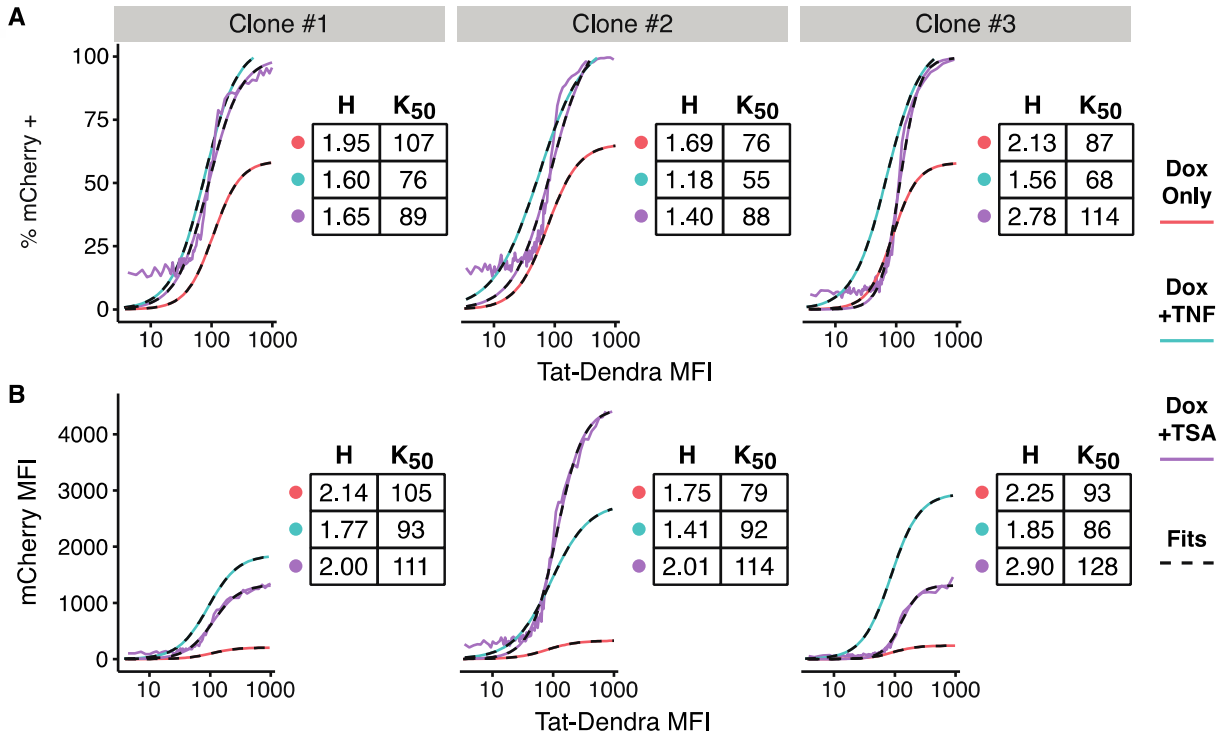

Figure S6: The non-physiological activator TSA and the cytokine TNF have distinct effects on threshold parameters. (A) Dose-response curves for %mCherry positive cells from flow cytometry measurements of three isoclones of Jurkat Tet-Tat-Dendra + LTR-mCherry, at 20 hours post Dox induction in the presence of TSA (trichostatin A, a histone deacetylase inhibitor). Each data point depicts a group of 500 cells. These data were fit to a Hill function (dashed lines), with Hill coefficient (*H*) and half-maximal binding (K_{50}) values in adjacent table. Hill fits from Fig. 4 are presented for comparison. (B) Dose-response curves from the above experiment, showing mCherry MFI. While TNF consistently decreases *H* and K_{50}, TSA has a less consistent effect on both parameters.

Mathematical Modeling Appendix

Based on previous literature (Ha and Ferrell, 2014), we explored a number of different models in an attempt to recapitulate the threshold response observed in the data. We began by examining previous models (Weinberger and Shenk, 2007) with acetylation de-acetylation cycles in Tat feedback, since such enzymatic 'futile cycles' can lead to ultrasensitive responses udner certain conditions (Ha and Ferrell, 2014). We exmaine these models in both the steady-state and pre-steady-state regime. For simplicity, we examine highly course-grained models where transcription and translation processes are represented by lumped parameters.

■ Reversible Acetylation of Tat (analysis of model from Weinberger & Shenk, *PLoS Biol.* 2007)

In this model, Tat is expressed in an deacetylated form (Tat_d) and can be acetylated at lysinses (the K50 or K51 residues) to produce acetylated Tat (Tat_A) that is required for transactivation of the LTR promoter to ultimately produce mCherry (transcription and translation are represented by lumped parameters).

$$\left(\begin{array}{c} \frac{d\,\text{Tat}_d(t)}{\text{dt}} = \beta - k_A\,\text{Tat}_d(t) + k_d\,\text{Tat}_A(t) - \delta_{\text{tat}}\,\text{Tat}_d(t) \\ \frac{d\,\text{Tat}_A(t)}{\text{dt}} = k_A\,\text{Tat}_d(t) - k_d\,\text{Tat}_A(t) \\ \frac{d\,\text{mCherry}(t)}{\text{dt}} = \alpha\,\text{Tat}_A(t) - \delta_{\text{mch}}\,\text{mCherry}(t) \end{array}\right)$$

Where β is the lumped rate of dox-induced Tat production, k_A and k_d, are the rates of Tat acetylation and deacetylation, respectively, α is the lumped rate of mCherry production, based on acetylated Tat transctivation of the LTR, and δ_{tat} and δ_{mch} are the per capita protein decay rates for mCherry and Tat, respecitvely. The steady states can easily be solved:

$$\left(\overline{\text{Tat}_A} \to \frac{\beta\,k_A}{k_d\,\delta_{\text{tat}}} \quad \overline{\text{Tat}_d} \to \frac{\beta}{\delta_{\text{tat}}} \quad \overline{\text{mCherry}} \to \frac{\alpha\,\text{Tat}_A}{\delta_{\text{mch}}}\right)$$

and a straightforward algebraic rearrangement shows that mCherry's steady state scales as a linear function of the Tat_d steady state. This can also be seen by plotting mCherry as a function of Tat using a parametric plot in *Mathematica*™ (using the parameters $\{\alpha \to 10,\ k_A \to 0.01,\ k_d \to 1,\ \delta_{\text{tat}} \to 0.25,\ \delta_{\text{mch}} \to 0.2\}$ and allowing β to vary between [0,20])

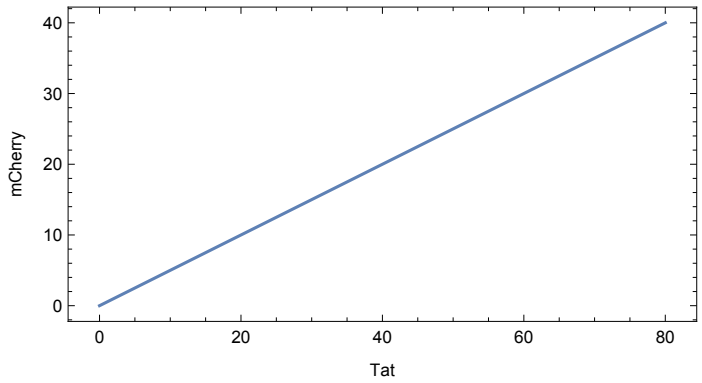

This simple model can be analytically solved in the pre-steady-state regime (and plotted using the parameter estimates above):

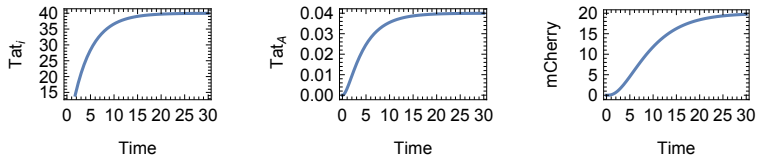

This analytical solution allows analysis of mCherry vs. Tat in the pre-steady-state regime using the parametric plotting function in *Mathematica* (β varying from [0,10] in this case):

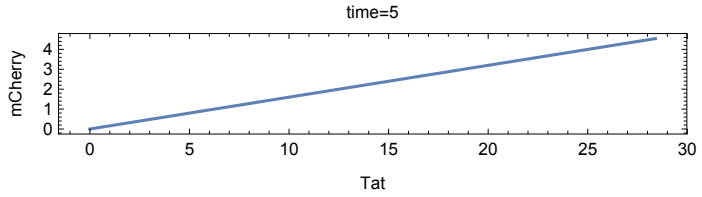

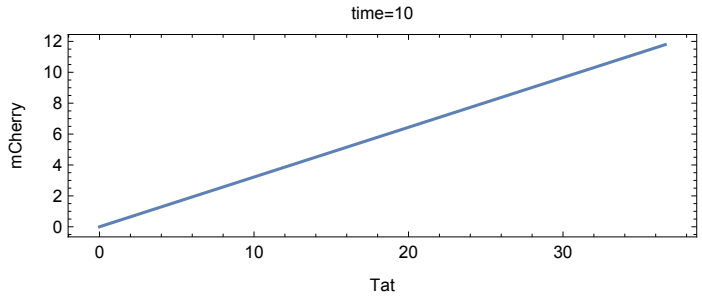

Clearly, this model does not generate a threshold response in either the steady-state or pre-steady-sate regime.

▫ *Saturable version of 2007 model*

Since the above model uses mass-action kinetics for acetylation and well-known examples of ultrasensitivty depend on conversion reactions being in the saturated (non mass action) zero-order regime (Ha and Ferrell, 2014), we also explored a saturable version of this model:

$$\frac{d\,\mathrm{Tat}_d(t)}{dt} = \frac{k_d\,\mathrm{Tat}_A(t)}{\mathrm{Tat}_A(t)+k_M} - \frac{k_A\,\mathrm{Tat}_d(t)}{\mathrm{Tat}_d(t)+k_M} + \beta - \delta_{\mathrm{tat}}\,\mathrm{Tat}_d(t)$$

$$\frac{d\,\mathrm{Tat}_A(t)}{dt} = \frac{k_A\,\mathrm{Tat}_d(t)}{\mathrm{Tat}_d(t)+k_M} - \frac{k_d\,\mathrm{Tat}_A(t)}{\mathrm{Tat}_A(t)+k_M}$$

$$\frac{d\,\mathrm{mCherry}(t)}{dt} = \frac{\alpha\,\mathrm{Tat}_A(t)}{\mathrm{Tat}_A(t)+k_M} - \delta_{\mathrm{mch}}\,\mathrm{mCherry}(t)$$

which yields steady states:

$$\left(\begin{array}{c} \mathrm{Tat}_A \to -\frac{\beta\,k_A}{\beta\,k_A-\beta\,k_d-k_d\,\delta_{\mathrm{tat}}} \\ \mathrm{Tat}_d \to \frac{\beta}{\delta_{\mathrm{tat}}} \\ \mathrm{mCherry} \to -\frac{\alpha\,\beta\,k_A}{\delta_{\mathrm{mch}}\,(\beta\,k_A-\beta\,k_d-k_d\,\delta_{\mathrm{tat}})} \end{array}\right)$$

but which still generates a hyperbolic response in steady state as visualized by a parametric plot (with $k_M = 1,\ \alpha = 100,\ \beta$ varied from $[0,\ 20]$ and other parameters as above):

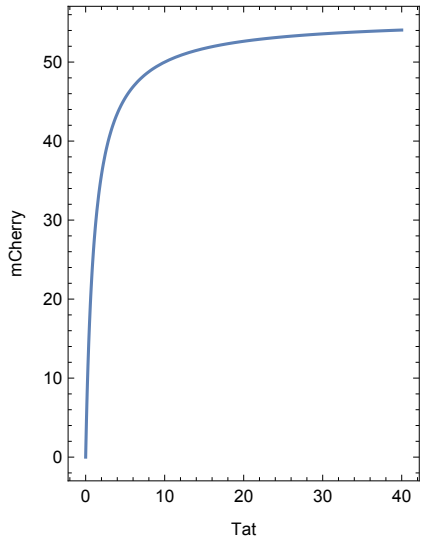

Numerical solutions of this model also generate a hyperbolic dose-response functions in the pre-steady-state regime as plotted using a numerical parametric plotting function (β varied from [0,20] all other parameters as above):

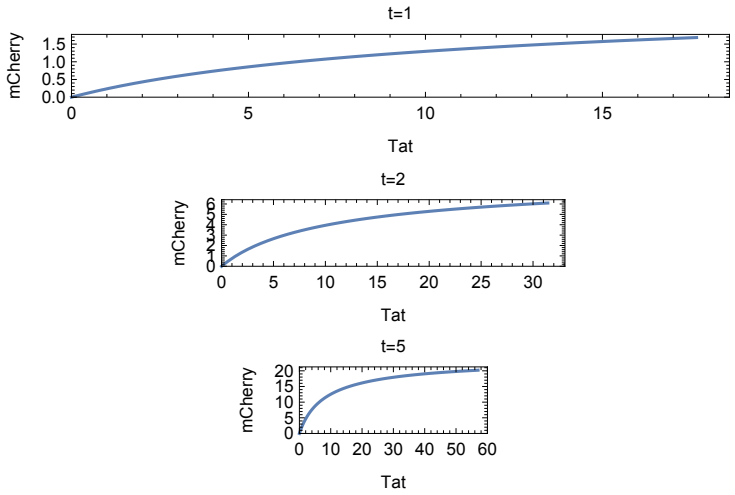

■ Multi-site Reversible Acetylation of Tat

We also explored an extended model with additional acetylation steps:

$$\frac{d\,\mathrm{Tat}_d(t)}{dt} = k_d\,\mathrm{Tat}_A(t) - k_A\,\mathrm{Tat}_d(t) + \beta - \delta_{\mathrm{tat}}\,\mathrm{Tat}_d(t)$$

$$\frac{d\,\mathrm{Tat}_A(t)}{dt} = -k_d\,\mathrm{Tat}_A(t) + k_A\,\mathrm{Tat}_d(t) - k_A\,\mathrm{Tat}_A(t) + k_d\,\mathrm{Tat}_{\mathrm{A2}}(t)$$

$$\frac{d\,\mathrm{Tat}_{\mathrm{A2}}(t)}{dt} = k_A\,\mathrm{Tat}_A(t) - k_d\,\mathrm{Tat}_{\mathrm{A2}}(t)$$

$$\frac{d\,\mathrm{mCherry}(t)}{dt} = \alpha\,\mathrm{Tat}_{\mathrm{A2}}(t) - d_{\mathrm{mch}}\,\mathrm{mCherry}(t)$$

which yields the following steady states:

$$\left(\begin{array}{c} \mathtt{Tat_A} \to \frac{\beta\,\mathtt{k_A}}{\mathtt{k_d}\,\delta_{\mathtt{tat}}} \\ \mathtt{Tat_d} \to \frac{\beta}{\delta_{\mathtt{tat}}} \\ \mathtt{Tat_{A2}} \to \frac{\beta\,\mathtt{k_A^2}}{\mathtt{k_d^2}\,\delta_{\mathtt{tat}}} \\ \mathtt{mCherry} \to \frac{\alpha\,\beta\,\mathtt{k_A^2}}{\mathtt{k_d^2}\,\delta_{\mathtt{mch}}\,\delta_{\mathtt{tat}}} \end{array}\right)$$

which, as above, show that the dose-response of mCherry is linear with respect to Tat_d and shows implicitly that increasing the number of acetylation sites will not change the linear response to Tat (since the nonlinearity appears only in the rate constants k_A and k_d not in other parameters). For completeness, we show that plots of the steady-states response of this model yielded a hyperbolic dose-response function at steady state as visualized by a parametric plot:

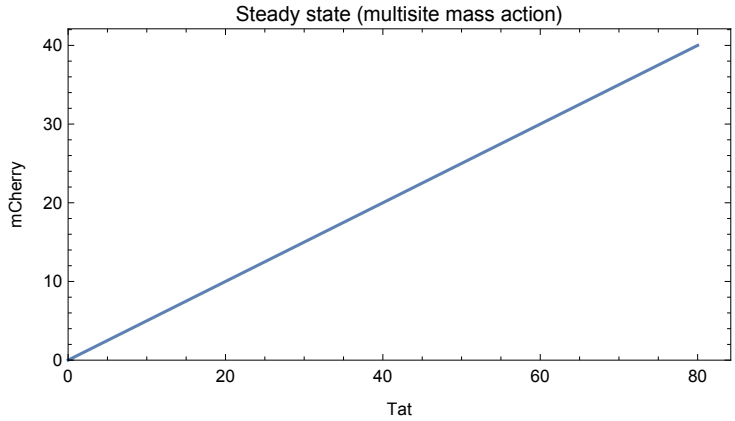

We also examined the pre-steady-state regime for this multi-site acetylation model and found that it also yields hyperbolic dose-response function (all parameters as above)

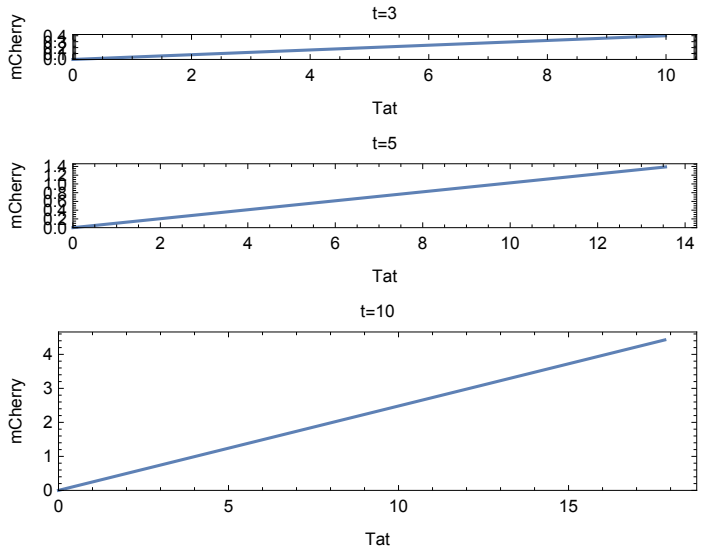

▫ *Saturable version of Multi-site Reversible Acetylation of Tat*

The saturable version of this model:

$$\frac{d\,\mathrm{Tat}_d(t)}{dt} = -\frac{k_A\,\mathrm{Tat}_d(t)}{\mathrm{Tat}_{id}(t)+1} + \frac{k_d\,\mathrm{Tat}_A(t)}{\mathrm{Tat}_A(t)+1} + \beta - \delta_{\mathrm{tat}}\,\mathrm{Tat}_i(t)$$

$$\frac{d\,\mathrm{Tat}_A(t)}{dt} = -\frac{k_d\,\mathrm{Tat}_A(t)}{\mathrm{Tat}_A(t)+1} + \frac{k_A\,\mathrm{Tat}_d(t)}{\mathrm{Tat}_d(t)+1} - \frac{k_A\,\mathrm{Tat}_A(t)}{\mathrm{Tat}_A(t)+1} + \frac{k_d\,\mathrm{Tat}_{A2}(t)}{\mathrm{Tat}_{A2}(t)+1}$$

$$\frac{d\,\mathrm{Tat}_{A2}(t)}{dt} = \frac{k_A\,\mathrm{Tat}_A(t)}{\mathrm{Tat}_A(t)+1} - \frac{k_b\,\mathrm{Tat}_{A2}(t)}{\mathrm{Tat}_{A2}(t)+1}$$

$$\frac{d\,\mathrm{mCherry}(t)}{dt} = \frac{\alpha\,\mathrm{Tat}_{A2}(t)}{\mathrm{Tat}_{A2}(t)+1} - \delta_{\mathrm{mch}}\,\mathrm{mCherry}(t)$$

Yields steady states:

$$\left(\begin{array}{c} \mathrm{Tat}_A \to -\frac{k_A\,\mathrm{Tat}_d\,k_M}{k_A\,\mathrm{Tat}_d - k_b\,\mathrm{Tat}_d - k_b\,k_M} \\ \mathrm{Tat}_i \to \frac{\beta}{\delta_{\mathrm{tat}}} \\ \mathrm{Tat}_{A2} \to -\frac{k_A^2\,\mathrm{Tat}_d\,k_M}{k_A^2\,\mathrm{Tat}_d - k_b^2\,\mathrm{Tat}_d - k_b^2\,k_M} \\ \mathrm{mCherry} \to -\frac{\alpha\,k_A^2\,\mathrm{Tat}_d\,k_M}{\delta_{\mathrm{mch}}\left(k_A^2\,\mathrm{Tat}_d - k_b^2\,\mathrm{Tat}_d - k_b^2\,k_M\right)} \end{array}\right)$$

which produced a qualitatively similar hyperbolic response in the steady-state regime that can be visualized by a parametric plot (α=100, β varied from [0,20], and other parameters as above):

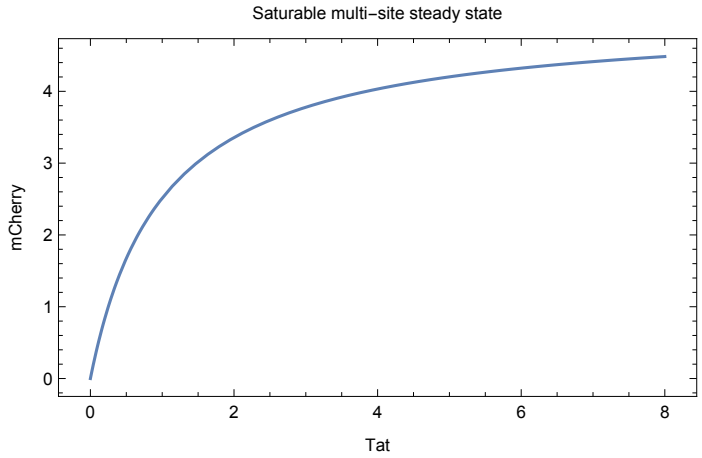

and the pre-steady-state regime (parameters as above):

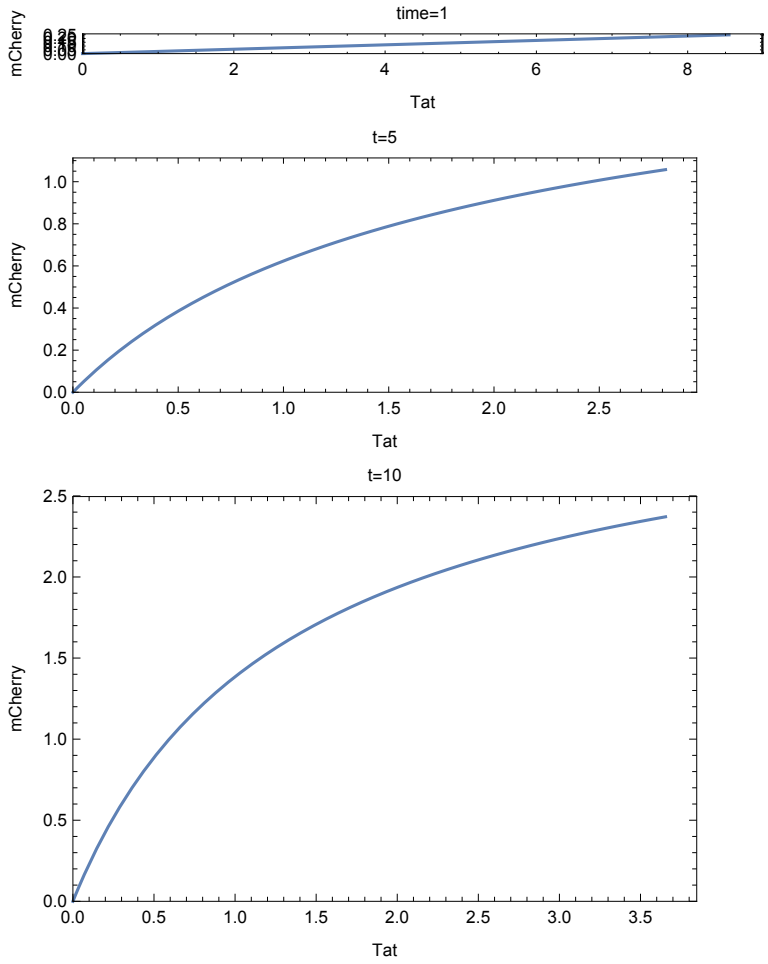

Overall, these results show that in the deterministic regime, models incoporating reversible covalent modifications of Tat (with either mass action or saturable kinetics) could not recapitulate the threshold response.